OH 231.8+4.2: its energetic bipolar outflow and rich chemistry

C. Sánchez Contreras[1], V. Bujarrabal and J. Alcolea

Observatorio Astronómico Nacional (IGN), Ap. 1143, E-28800 Alcalá de Henares, Spain

Luis F. Miranda

Instituto de Astrofísica de Andalucía, CSIC, Ap. 3004, C/ Sancho Panza s/n, E-18080 Granada, Spain

J. Zweigle

German Aerospace Center (DLR), Institute of Optoelectronics, 82230 Wessling, Germany

Abstract. We report results from observations taken at different wavelengths (optical, radio and NIR) of the bipolar Protoplanetary Nebula OH 231.8+4.2. Radio interferometry with high spatial resolution has been particularly revealing. We study the complex structure and dynamics of this object as well as its rich chemistry.

1. Introduction

OH 231.8+4.2 (hereafter OH 231.8) is a well studied source presumably in transition between the AGB and the planetary nebula (PN) phase. This object is unique, due to its large angular extent, for studying the complex dynamics present in this kind of objects. Like most protoplanetary nebulae (PPNe), OH 231.8 has a clear bipolar morphology. In the visible it shows two lobes emerging from an obscured region where the central star lies (Reipurth 1987). Herbig-Haro-like objects have been observed beyond the lobes (Cohen et al. 1985), which are attributed to the post-AGB wind interaction phenomenon. OH 231.8 is classified as an O-rich source, in view of its SiO, OH, and H_2O maser emission (Bowers & Morris 1984, and references therein). Also, emission from a large variety of C-bearing molecules has been detected in this source. The presence of a Mira variable in the heart of OH 231.8 has been recently confirmed by direct imaging in the NIR (Kastner et al. 1998), the central star being classified as M9 III (Cohen et al. 1981). However, the detection of a blue excess in the optical continuum could suggest the presence of a hotter companion (Cohen et al. 1985).

---

[1] Also Departamento de Astrofísica, F. C. Físicas, U. Complutense, E-28040 Madrid, Spain
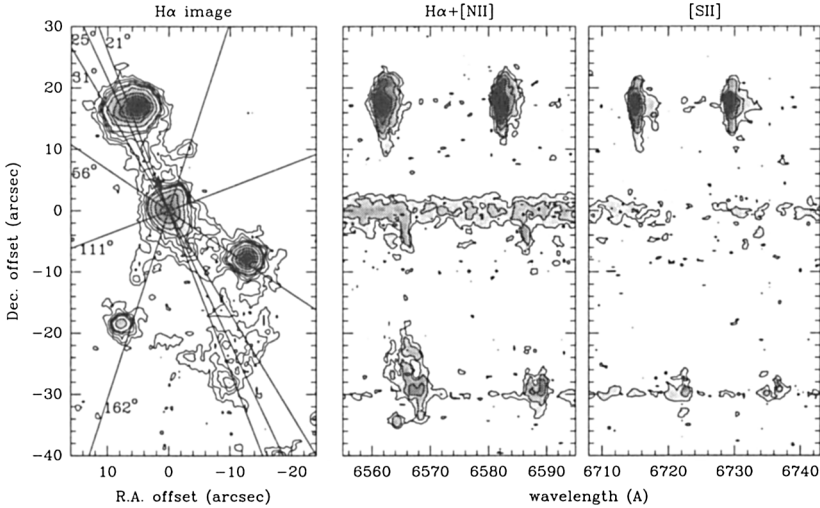
347

Figure 1.   Hα image and long-slit Hα, [NII] and [SII] spectra along the symmetry axis of OH 231.8+4.2

2.   Optical long-slit spectroscopy of OH 231.8+4.2

We have obtained long-slit spectra of OH 231.8 using the IDS spectrograph of the 2.5 m Isaac Newton Telescope of the Roque de los Muchachos Observatory (Canary Islands, Spain). Six slit positions were observed at position angles 21° (the symmetry axis of the object), 25°, 31°, 56°, 111° and 162°, (see Fig. 1). We have detected the main nebular lines (Hα, [NII] 6548+6583, [SII] 6716+6731, [OI] 6300+6363, [OII] 3726+3729, [OIII] 4959+5007 and Hβ).

In Fig. 1 we show the Hα, [NII] and [SII] spectra for the 21° slit (symmetry axis). Note the wide profiles of the lines, with a total projected velocity range of ~ 500 km s^{-1}. The emission from the North/South lobe is blue/red-shifted. This fact indicates that the gas is flowing outwards, since the North lobe is the nearest of the two. The axial velocity gradient present in OH 231.8 is ~ 5 km s^{-1} arcsec^{-1}. This value provides a direct measurement of the kinematic age of the lobes, of about 1 000 yr, in agreement with previous estimations of the time spent in the PPN phase. We have assumed an inclination of the nebula with respect to the plane of the sky of 40°, and a distance of 1 500 pc (Bowers & Morris 1984; Kastner et al 1992). The complexity of the kinematics and of the structure of the lobes is remarkable. Particularly, part of the gas in the South lobe seems to expand like a bubble (see the nearly elliptical spectral feature at the end of the South lobe on the Hα spectrum, Fig. 1). We suggest that such a bubble-like structure is originated by the shock-accelerated gas moving outward and its backward countershock. On the other hand, we have found intense emission from forbidden lines of [NII], [SII] and [OIII] which demonstrates the shocked nature of the line emitting gas in the lobes of OH 231.8. In the long-slit spectra in Fig. 1, we can also see the stellar continuum reflected by the nebula. The detailed study of such a spectrum confirms the M9 III type of the central

star. From the [SII] $\lambda 6716$/[SII] $\lambda 6731$ lines ratio we have estimated the average electron density in the lobes of OH 231.8, which ranges between 400 cm^{-3} (North Lobe) and $\lesssim 100$ cm^{-3} (South Lobe). We find that the total ionized mass of the nebula is of the order of 10^{-4} $M_{\odot}$.

3. Structure and kinematics of the neutral envelope of OH 231.8+4.2

In order to study the neutral envelope of OH 231.8, and not only the relatively highly excited component traced by the previous optical observations, we have carried out single-dish and interferometric maps at millimeter wavelengths of different molecular lines. We have used the IRAM 30 m radiotelescope (Granada, Spain) and the Plateau de Bure interferometer (French Alps). The observed transitions are: ^{12}CO and ^{13}CO (J=1–0 and J=2–1), HCO$^+$ (J=1–0), HCN (J=1–0), HNC (J=1–0), SO ($J=2_2$–1_1), SO$_2$ ($J=10_{0,10}$–$9_{1,9}$), CS (J=5–4), H^{13}CN (J=1–0), SiO (J=5–4), SiO maser (v=1 J=2–1) and NS ($^2\Pi_{1/2}$, J=5/2–3/2). For ^{12}CO, the best tracer of the total mass, we have performed 3-point mosaicing, interferometric observations to properly study the mass distribution in the whole nebula.
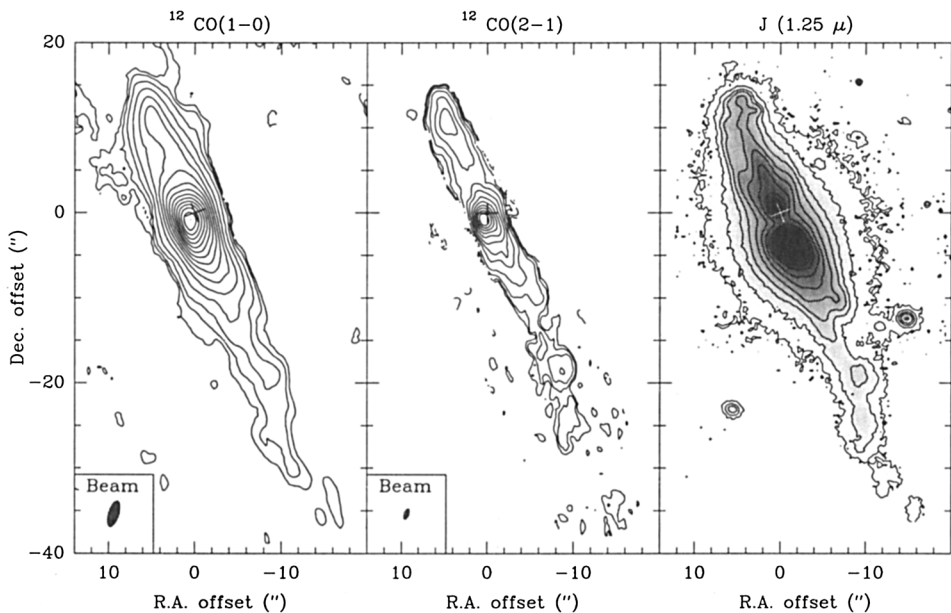

Figure 2. Integrated intensity ^{12}CO maps and J image of OH 231.8+4.2. Levels are: 1, 2.5, 5, 10 to 100 by 10% for the CO maps, and 0.2, 0.4, 0.75, 1.25, 2.5, 5, 10 to 100 by 10% for the J image

In Fig. 2 we show the integrated intensity maps of ^{12}CO. We find that the emission is very extended and narrow ($\sim 55'' \times 4''$). Note also the asymmetry with respect to the equator and the clumpiness of the nebula, which, in fact, consists of different mass condensations. Another good tracer of the mass, independently of the excitation, is the NIR emission. Such an emission arises from

reflected light by dust grains and outlines the mass distribution, except for the center where there is a large extinction. We have obtained maps at different NIR bands (J, H and K') using the IRAC-2b camera of the 2.2 m ESO Telescope (La Silla, Chile). In Fig. 2 we show the J image. Note the agreement between both the CO and J maps. The total axial extent is very similar in both maps, the J map also showing an undulating tail of material toward the South and a clear clumpy structure. The different distributions of the neutral and of the high-excitation components are remarkable (Figs. 1 and 2). In the direction perpendicular to the nebula axis, the atomic gas is much more extended than the CO gas which seems to be confined to the axis. The extent in the axial direction is very similar in both cases.

The very wide CO profiles (~ 330 km s^{-1}, projected) indicate the presence of a high-velocity molecular flow in OH 231.8. We find a displacement of the emitting regions along the axis for the different velocity intervals, so that the red-and blueshifted emissions arise from the South and North lobe, respectively. In Fig. 3 we show the interferometric velocity-position diagrams along the symmetry axis for ^{12}CO and other two representative molecules. For all the molecular lines we find a similar emission distribution (that from CO being the most extended) and kinematics, except for HCO$^+$ (see below). We have found a strong velocity gradient along the nebula axis, which is in general compatible with that of the high-excitation component. We stress on the high velocities reached by the neutral material at the end of the lobes of OH 231.8. We think that the acceleration of the lobes must be due to the interaction between the fast, post-AGB ejections and the slow, circumstellar envelope originated during the red giant phase. In all the molecules, we find a relatively narrow component at the systemic velocity located at the nebula center, so it could be the remnant of the AGB envelope which has not been accelerated by the fast post-AGB ejections.

4. OH 231.8+4.2: mass, momentum and abundances

We have calculated the mass, momentum and abundances of the different clumps of OH 231.8. The method followed is described in detail in Sánchez Contreras et al. (1997). For simplicity, we have chosen six different clumps related to six velocity intervals (indicated in the tables) corresponding to the different features found in both our line profiles and spatial intensity distributions.

In the estimation of the mass from the ^{13}CO(1-0) line, we have assumed that it is optically thin, and a standard value for the ^{13}CO abundance in AGB envelopes. The excitation state has been estimated from the ^{12}CO(2-1)/^{12}CO(1-0) brightness temperature ratio. We have found such a ratio to be almost constant along the axis, giving a value for the rotational temperature of about 10 K. Note that such a low temperature suggests a strong cooling after the post-AGB shock.

In Table 1 we show the mass, the average (deprojected) velocity with respect to the systemic velocity, and the momentum associated to the different velocity intervals or clumps. We have found a total mass $\sim 0.6~M_\odot$, of which at least $0.2~M_\odot$ are flowing at high velocity. These values can be underestimated, probably not more than a factor 2, but not significantly overestimated (see discussion in Sánchez Contreras et al. 1997). Our mass estimations are compatible
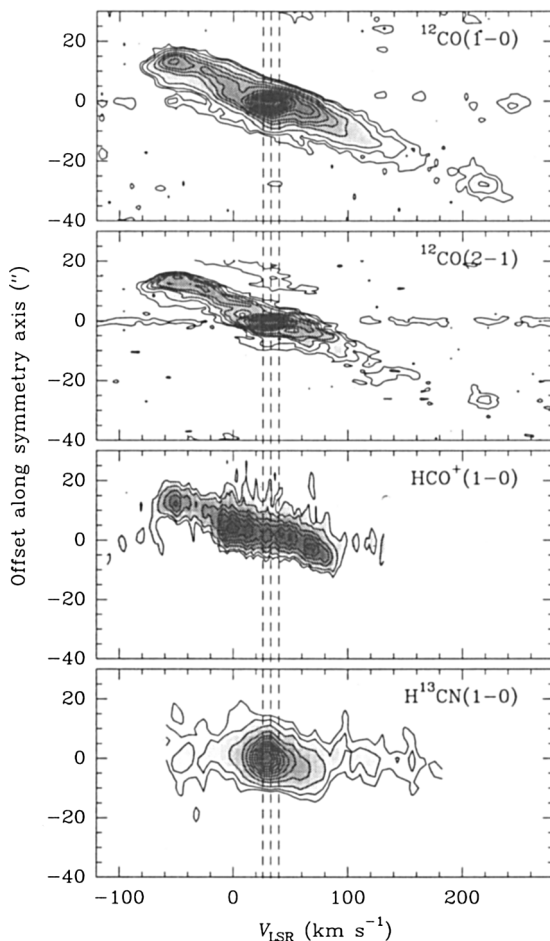
Figure 3. IRAM Plateau de Bure velocity-position maps along the symmetry axis of OH 231.8+4.2 in some of the observed transitions

with the total dust mass in OH 231.8, $\sim 0.01\ M_\odot$ (Kastner et al. 1995), which leads to a molecular mass of about 1 $M_\odot$ if we assume a standard value for the gas-to-dust ratio. We have also estimated the mass-loss during the last AGB phases ($\sim 10^{-4}\ M_\odot\ \mathrm{yr}^{-1}$). We have found very high values for the momentum carried by the gas in the lobes, in both of about 10 $M_\odot\ \mathrm{km\,s}^{-1}$. If the radiation pressure was the only mechanism responsible from the momentum increase, then the interaction time should have been $\sim 50\,000\,\mathrm{yr}$. This time is, however, extremely large compared with the expected value, which must be a small fraction of the PPN stage duration ($\sim 1\,000\,\mathrm{yr}$). Even if we consider a strong effect of multiple scattering, we need another additional mechanism to produce such high momentum.

In Table 2 we show the derived abundances of the different species observed in the different clumps of OH 231.8. We assumed that all lines are optically thin

Table 1.   Mass and momentum of the clumps

	interval $\mathrm{km\,s^{-1}}$ (LSR)	mass $(M_\odot)$	V_i $(\mathrm{km\,s^{-1}})$	momentum $(M_\odot\,\mathrm{km\,s^{-1}})$
I1	−80:−30	0.04	137	5.5
I2	−30:+10	0.11	67	7.4
I3	+10:+55	0.29		
I4	+55:+80	0.08	54	4.3
I5	+80:+150	0.03	128	3.8
I6	+150:+250	0.01	260	2.6

Table 2.   Molecular abundances for the clumps

interval $\mathrm{km\,s^{-1}}$ (LSR)	−80:−30	−30:+10	+10:+55	+55:+80	+80:+150	+150:+250
$X(HCO^+)$	$1.3\ 10^{-8}$	$1.3\ 10^{-8}$	$3.5\ 10^{-9}$	$1.0\ 10^{-8}$	$1.4\ 10^{-8}$	$< 2.5\ 10^{-8}$
$X(SiO)$	$0.9\ 10^{-8}$	$1.8\ 10^{-8}$	$1.7\ 10^{-8}$	$1.2\ 10^{-8}$	$1.1\ 10^{-8}$	$\lesssim 1.0\ 10^{-8}$
$X(HNC)$	$0.6\ 10^{-8}$	$1.0\ 10^{-8}$	$2.1\ 10^{-8}$	$0.7\ 10^{-8}$	$1.0\ 10^{-8}$	
$X(H^{12}CN)$	$4.0\ 10^{-8}$	$3.6\ 10^{-8}$	$6.9\ 10^{-8}$	$5.2\ 10^{-8}$	$2.4\ 10^{-8}$	
$X(H^{13}CN)$		$3.6\ 10^{-9}$	$1.3\ 10^{-8}$	$6.1\ 10^{-9}$		
$X(CS)$	$0.6\ 10^{-7}$	$0.3\ 10^{-7}$	$0.8\ 10^{-7}$	$0.2\ 10^{-7}$	$0.4\ 10^{-7}$	$< 1.0\ 10^{-7}$
$X(SO_2)$		$0.2\ 10^{-5}$	$1.4\ 10^{-5}$	$1.1\ 10^{-5}$	$1.3\ 10^{-5}$	
$X(SO)$			$2.4\ 10^{-6}$			

and the masses of the clumps previously estimated. We also assumed the same rotational temperature (10 K) in all cases. The most interesting result from these calculations is the very strong decrease in the central clump of the HCO^+ abundance, that is about 3 or 4 times lower than in the outer parts of the nebula. Moreover, the HCO^+ abundance is relatively high. Our results suggest that the efficient formation of this molecule in OH 231.8 is due to shock chemistry, since the HCO^+ emission appears particularly intense in the shock-accelerated lobes, and not in the central clump where one expects the maximum photoionization. The high abundance of SiO and SO_2 at relatively large distances from the center can also be due to the extraction of SiO and S from dust grains by shocks.

References

Bowers P.F., Morris M., 1984, ApJ 276, 646
Cohen M., 1981, PASP 93, 288
Cohen M., Dopita M.A., Schwartz R.D., Tielens A.G.G.M., 1985, ApJ 297, 702
Kastner J.H., Weintraub D.A., Zuckerman B., et al., 1992, ApJ 398, 552
Kastner J.H., Weintraub D.A., 1995, AJ 109, 1211
Kastner J.H., Weintraub D.A., Merril K.M., Gatley I., 1998, AJ 116, 1412
Reipurth B., 1987, Nature 325, 787
Sánchez Contreras C., Bujarrabal V., Alcolea J., 1997, A&A 327, 689